Received: 11 October 2021 | Revised: 12 June 2022 | Accepted: 2 September 2022

DOI: 10.1002/met.2099

Meteorological Applications
Science and Technology for Weather and Climate
Open Access
RMetS

RESEARCH ARTICLE

A delayed modulation of solar ultraviolet radiation on the COVID-19 transmission reflects an incubation period

Maosheng He[1] | **Keyan Fang**[2,3] | **Feifei Zhou**[2] | **Tinghai Ou**[3] | **Deliang Chen**[3]

[1]Kuehlungsborn, Germany

[2]Key Laboratory of Humid Subtropical Eco-Geographical Process (Ministry of Education), Fujian Normal University, Fuzhou, China

[3]Regional Climate Group, Department of Earth Sciences, University of Gothenburg, Gothenburg, Sweden

Correspondence
Keyan Fang, Key Laboratory of Humid Subtropical Eco-Geographical Process (Ministry of Education), Fujian Normal University, Fuzhou 350007, China.
Email: kujanfang@gmail.com

Funding information
National Natural Science Foundation of China, Grant/Award Numbers: 41822101, 41888101, 41971022; Swedish Formas, Grant/Award Number: 2017-01408; Strategic Priority Research Program of the Chinese Academy of Sciences, Grant/Award Number: XDB26020000

Abstract

Laboratory experiments have revealed the meteorological sensitivity of the coronavirus disease 2019 (COVID-19) virus. However, no consensus has been reached about how outdoor meteorological conditions modulate the virus transmission as it is also constrained by non-meteorological conditions. Here, we identify the outbreak's evolution stage, constrained least by non-meteorological conditions, by searching the maximum correlation coefficient between the ultraviolet flux and the growth rate of cumulative confirmed cases at the country level. At this least-constrained stage, the cumulative cases count around 1300–3200, and the count's daily growth rate correlates with the ultraviolet flux and temperature significantly (correlation coefficients $r = -0.54 \pm 0.09$ and -0.39 ± 0.10 at $p < 0.01$, respectively), but not with precipitation, humidity, and wind. The ultraviolet correlation exhibits a delay of about 7 days, providing a meteorological measure of the incubation period. Our work reveals a seasonality of COVID-19 and a high risk of a pandemic resurgence in winter, implying a need for seasonal adaption in public policies.

KEYWORDS

COVID-19, incubation period, transmission, ultraviolet flux

1 | INTRODUCTION

A way to predict the coronavirus disease 2019 (COVID-19) transmissions in winter is to quantify the responses of the virus survival and transmission to the winter weather conditions. Laboratory experiments revealed that ultraviolet (UV) radiation and air temperature modulate the airborne survival of the virus strongly (Ratnesar-Shumate et al., 2020; Schuit et al., 2020; Ujiie et al., 2020). Meanwhile, several studies have attempted to extract relevant epidemiological evidence (Iqbal et al., 2020; Qi et al., 2020; Sajadi et al., 2020; Ujiie et al., 2020; Yao et al., 2020) by studying the correlations between the count of confirmed cases or mortality and meteorological conditions using data from priorly selected cities. Their conclusions, however, are often contradictory. Some attempts did not find the correlation (Ujiie et al., 2020; Yao et al., 2020), whereas the others reported weak or moderate correlations (Iqbal et al., 2020; Qi et al., 2020; Sajadi et al., 2020). The results are not conclusive, mainly because the transmission is constrained by non-meteorological factors that can hardly be considered in an appropriate way.

Maosheng He and Keyan Fang contributed equally to this study.

At the early stage of an uncontrolled outbreak, the infection cases grow exponentially, whereas its growth rate is relatively stable (Hunt, 2014; Maier & Brockmann, 2020; Picoli Junior et al., 2011). Accordingly, here we investigate the initial growth rate of the infection cases, expecting the growth rate is more susceptible to meteorological conditions than the infection cases. However, at the early stage of an outbreak, the infection cases might not be confirmed timely and accurately as constrained potentially by insufficient test capability. On the other hand, at the late stage of an outbreak, the growth rate of the infection will become relatively less susceptible to meteorological conditions as being mitigated after effective artificial (Anderson et al., 1992; Liu et al., 2020). Therefore, we aim to determine the outbreak's stage, which is late enough when the test capability is sufficient and is also early enough so that the growth rate has not been mitigated by artificial controllers. We term this stage as the least-constrained stage, and determine it through an optimization. The optimization is performed by maximizing the correlation coefficient between the confirmed cases' growth rate and meteorological conditions over the accumulative confirmed case count. The growth rate at the least-constrained stage is defined as the least-constrained growth rate, and its response to meteorological conditions is investigated statistically. As discussed below, the least-constrained growth rate reflects minimum contamination from non-meteorological factors, for example, test capability and artificial controls, and reveals meteorological modulations in detail.

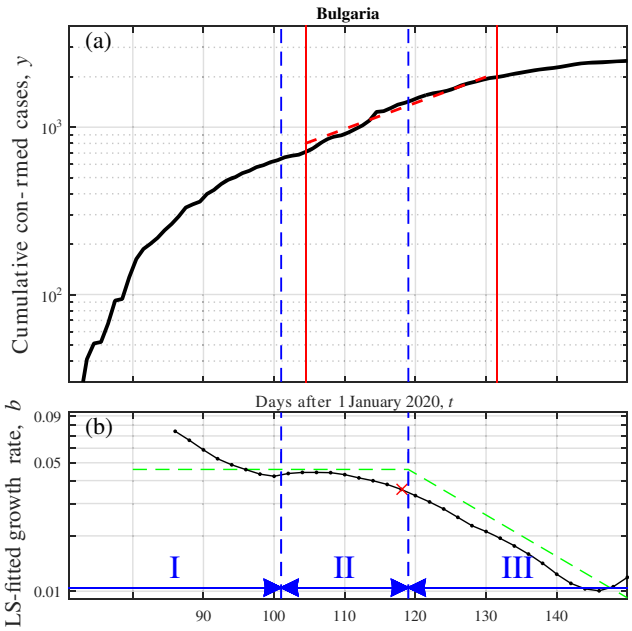

FIGURE 1 (a) Cumulative confirmed cases y as a function of time t and (b) its growth rate b against the regression time parameter τ, for Bulgaria as an example. The growth rate b (black line in (b)) is LS-fitted according to the model $y = ae^{b(t-\tau)}$ in a 28-day-wide sliding window centring at $\tau = 86, 88, ..., 152$, where a represents the model initial confirmed cases (namely, the LS-fitted y value at τ). The growth of confirmed cases could be divided into three stages: Stages I, II, and III, sketched by blue symbols in (b). In Stage II, the growth is stable ($0.035 < b < 0.045$), whereas in the other two, b decreases by more than 0.02. In Stages II and III but not in Stage I, the real growth is largely consistent with the ideal evolution that is sketched as the green line in (b) according to Liu et al., 2020; Anderson et al., 1992. We attribute the discrepancy in Stage I to an insufficient test capability at the early stage. The red symbols denote the least-constrained growth rate and its sampling window (see Sections 2.1–2.3 for details).

2 | DATA ANALYSES AND RESULTS

This study uses daily cumulative confirmed COVID-19 cases at a country level and daily meteorological variables until 1 September 2020. The confirmed cases are from COVID-19 Data Repository by the Center for Systems Science and Engineering at Johns Hopkins University, whereas the meteorological variables are extracted from the ERA5 reanalysis dataset from the European Centre for Medium-Range Weather Forecasts (C3S, 2017). The meteorological variables analysed herein include the air temperature at the height of 2 m above the surface (land, sea, or inland waters), precipitation, relative humidity, wind speed at the height of 10 m, downward UV radiation flux at the surface (UV, in the range of 250–440 nm), and diurnal temperature range. The daily mean meteorological data were averaged for each country to compare with the country-level COVID-19 data. Below, we compare the growth of confirmed cases with its theoretical expectation, in an example country in Section 2.1 and statistically in Section 2.2, determine the statistical stage modulated most sensitively by weather in Section 2.3, investigate the geographic distribution of the confirmed case growth and its correlation with meteorological factors in Sections 2.4 and 2.5, and diagnose the incubation period in Section 2.6.

2.1 | Evolution of the outbreak in an example country: Stages of the confirmed case growth

Figure 1a displays the cumulative confirmed case number y as a function of time t in Bulgaria as an example. Through a least-square (LS) regression, we fit y to an exponential model $y = ae^{b(t-\tau)}$ in a 28-day-wide sliding window. Here, $\tau = 86, 88, ..., 232$ days denotes the centre

of the sliding window, a measures the confirmed cases at the window centre τ, and the exponent factor b measures the growth rate. The LS-fitted growth rate b is shown in Figure 1b as a function of time. Besides b, the regression also results in a and r^2. a is the a LS estimation of y and r^2 measures the regression goodness equalling to the square of the correlation coefficient between $y(t)$ and its LS estimation. The LS-fitted growth rate b can be divided into three stages, labelled as I, II, and III and indicated by the blue arrows in Figure 1. Stages I and III are characterized by decreasing growth rates, whereas Stage II is associated with a relatively stable growth rate.

Theoretically, outbreaks of infectious diseases (Hunt, 2014; Maier & Brockmann, 2020; Picoli Junior et al., 2011) are characterized by two phases: the uncontrolled first phase showing stable exponential growth followed by a second phase with a decreasing growth rate usually after effective artificial controllers (Anderson et al., 1992; Liu et al., 2020). The two-phase theoretical growth is sketched as the green dashed line in Figure 1b, which is largely parallel to the growth of the confirmed case (black line) in Stages II and III, and can explain largely these stages. Stage II reflects the uncontrolled transmission of COVID-19, whereas Stage III reflects the decline phase where the decreasing growth rate could be explained as responses to artificial interventions or controllers, for example, travel restrictions and changes in human behaviours (Lai et al., 2020; Tian et al., 2020). However, in Stage I in Figure 1b, the black line is not parallel to the green. At the beginning of the outbreak, infections cannot be confirmed timely and can accumulate until sufficient tests. The decreasing growth rate of the confirmed case, biased from theoretical growth, might reflect more the delayed sufficient test capability than the infection growth.

Compared with Stages I and III, Stage II is characterized by a relatively stable growth rate reflecting uncontrolled transmissions confirmed timely and sufficiently. Therefore, we assume that in Stage II the growth is modulated most sensitively by the weather and will use Stage II for exploring the impacts of weather. In practice, the evolution of b exhibits dramatic morphological diversity between different countries. Instead of delimiting Stage II county by county, we investigate the evolution statistically in the following subsection.

2.2 | Statistical evolution of the outbreak

We implement the regression defined in the previous subsection on the cumulative confirmed cases from every country, yielding the LS-fitted confirmed case count a, the LS-fitted growth rate b, and the LS regression goodness r^2 as functions of τ. Figure 2a,b displays b against a and r^2 from the 50% most developed countries, respectively. These countries are characterized by the gross domestic product per capita 2019 above the median of all countries, 6200 United States dollars, and therefore are presumably least subject more to the socio-economic factors (Guha et al., 2020; Khalatbari-Soltani et al., 2020) as discussed further in Section 2.6 and detailed in Table S1. Figure 2b, b exhibits a dependence on r^2 at $r^2 < 0.9$. Accordingly, we exclude b values associated with $r^2 < 0.9$ from the following analyses. Here, r^2 quantifies how much of the total variance of the accumulative confirmed case y can be explained by our exponential model $y = ae^{b(t-\tau)}$. The high r^2 values reveal that the outbreak evolves exponentially.

Most studies on the evolution of accumulative confirmed case count typically used the date as the independent variable as we used in Figure 1. However, from a mathematical perspective, these two variables, the count and date, increase monotonically with each other. Therefore, alternatively, the count can also be denoted as the independent variable. In principle, both the count and date could be used to coordinate the growth rate in Figure 2a for comparing the evolution stages of the outbreaks in different countries. However, using the date entails shifting outbreaks in different countries to comparable phases and therefore entails determining the start of outbreak (namely, the concurrence of the first infection) or the start of comparable phases in all countries. Determining the concurrence of the first infection is subject to the uncertainty associated with, for example, the initial test capability, and determining comparable phases is potentially subject to prior knowledge or subjectively defined parameters. Both determinations might introduce errors and both require the confirmed case count anyway. To avoid these errors, we use the LS-fitted accumulative confirmed case count, a, rather than the date, t, as to coordinate the outbreak's evolution statistically.

In Figure 2a, the growth curve $b(a)$ does not clearly exhibit the three-stage shape of $b(\tau)$ in Figure 1b but looks more complicated. The curve minimizes at $a = 10^2$, $(1–2) \times 10^3$, 10^4 and 10^5, namely, integer powers of 10. Therefore, we conjecture they are unphysical but artificial signals, for example, data manipulation (Kapoor et al., 2020). Neglecting these minima, we divide largely the growth curve $b(a)$ into four stages. The final stage is characterized by a decreasing rate $b(a)$, corresponding to Stage III of the $b(\tau)$ growth in Figure 1b, and is labelled here also as Stage III. The other stages of $b(a)$ are labelled as I-, I, and II, respectively. Stage I- is associated with a small number of infections at the very beginning, and the growth might be susceptible to uncertainties and

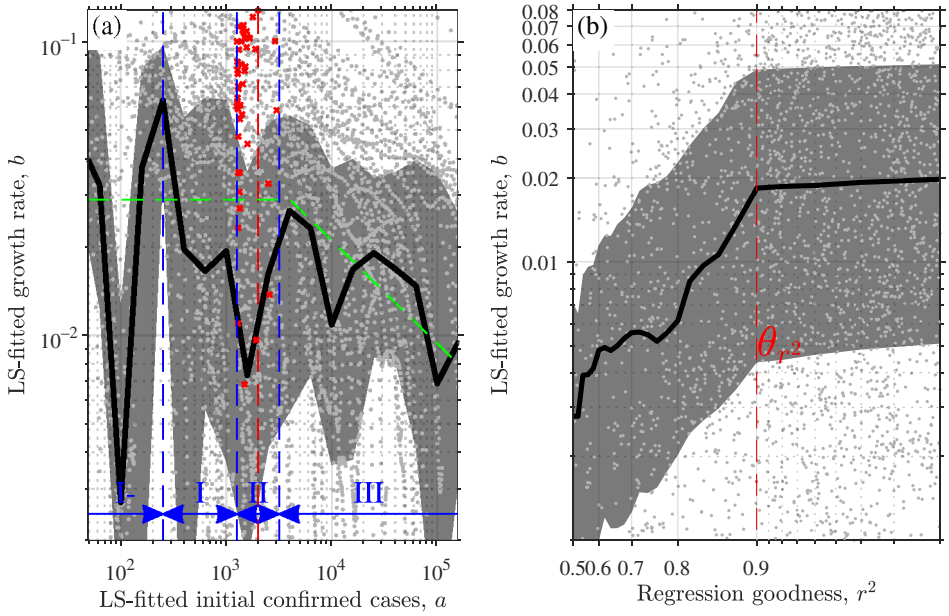

FIGURE 2 The growth rate b of the confirmed cases against (a) the LS-fitted initial confirmed cases a and (b) the goodness r^2 of the exponential regression as instanced in Figure 1. In each panel, one dot corresponds to one sliding step of the regression; and the bold black solid line and grey shadow illustrate the median and the interquartile range, respectively. In (a), the green line sketches the ideal evolution according to Anderson et al. (1992); the blue symbols sketch different Stages of the evolution of the outbreak among which Stages I, II, and III are the statistical estimations of Stages I, II, and III instanced in Figure 1. Stage II is centring at the red dashed line $a_c = 2000$, determined in Section 2.3. In (a), the red crosses denote the least-constrained growth rate b_m, namely, the maximum b in Stage II for each country. In (b), the red line displays the threshold value $\theta_{r^2} = 0.9$ in (b) used in selecting b_m. See Section 2.2 for the details.

therefore is excluded from the following analyses. Stage I is characterized largely by a decreasing growth rate $b(a)$, corresponding to Stage I of $b(\tau)$ in Figure 1b. We assume that $b(a)$ in-between Stages I and III correspond to Stage II in Figure 1b where the growth is relatively stable and reflects timely and sufficiently confirmed uncontrolled transmissions. Note that in Figure 1a, the range of Stage II is just a sketch, which is not determinative. We determine the statistical range of Stage II by searching the maximum correlation coefficient between meteorological factors and the growth rate in the following subsection, assuming that in Stage II the growth is modulated most sensitively by weather.

2.3 | The statistical stage modulated most sensitively by weather

The statistical Stage II can be denoted as $a_c \cdot S^{-1} < a < a_c \cdot S$ where S represents the half-width of the stage and a_c represents the stage centre. To start, we temporally assign $S = 10^{0.2}$ and $a_c = 10^2$ and define the first candidate of Stage II: $10^{1.8} < a < 10^{2.2}$. In this candidate range, we search the maximum $b(a)$ of each country, and calculate the correlation coefficient r_{UV} between the maximum $b(a)$ and the UV flux (as detailed in the following subsections) across all countries. Similarly, we calculate r_{UV} for other candidates of Stage II, including $10^{1.9} < a < 10^{2.3}$, $10^{2.0} < a < 10^{2.4}$, ..., and $10^{3.8} < a < 10^{4.2}$ (namely, the a range centres at $a_c = 10^{2.1}$, $10^{2.2}$, ..., and $10^{4.0}$ with a half-width $10^{0.2}$). The absolute value $|r_{\mathrm{UV}}|$ as a function of a_c is displayed as the solid blue line in

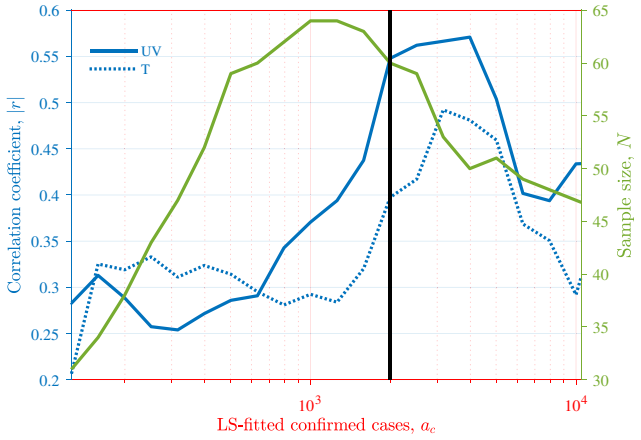

FIGURE 3 The absolute correlation coefficients $|r|$ (between b_m and two meteorological factors) and valid sampling size N as functions of a_c. The vertical black line at $a_c = 2000$ represents the a_c used for calculating the b_m in the current work. See Section 2.3 for the details.

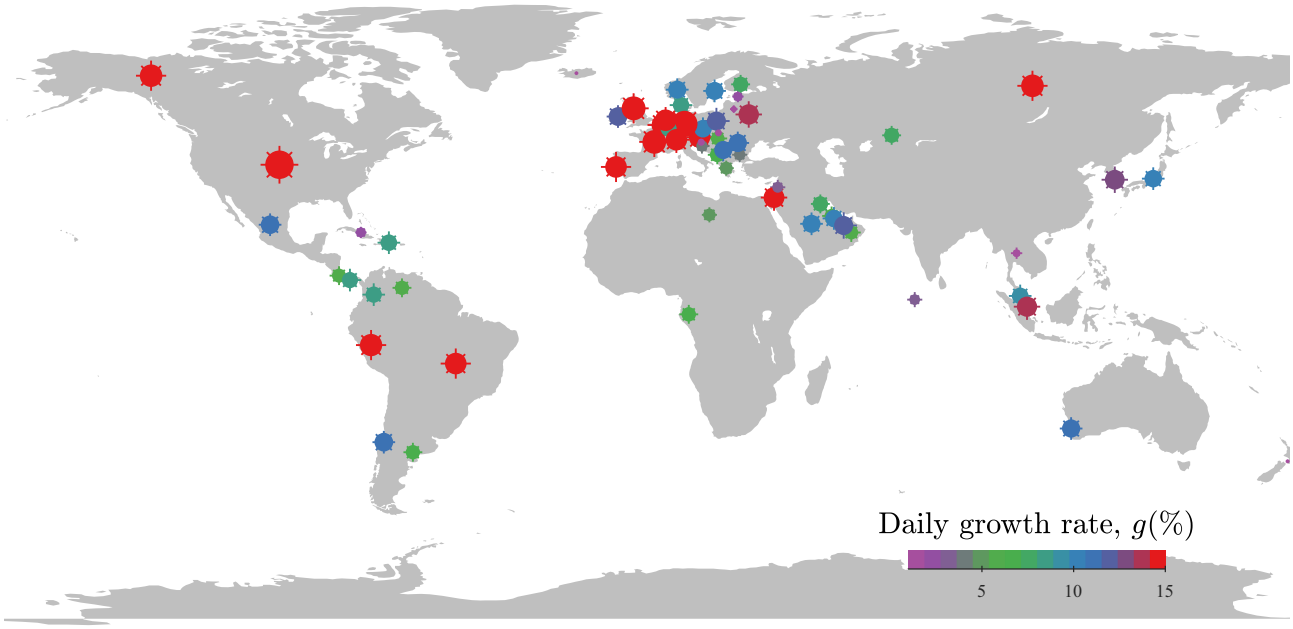

FIGURE 4 Global distribution of the daily growth rate g of COVID-19 confirmed cases. Each point represents one country/region. Both the colour and the size of the symbols represent the growth rate. The growth rate is estimated through a sliding window regression detailed in Section 2.1 and an optimization in Section 2.3. Here, only 50% of most developed countries are included (according to the gross domestic product per capita 2019).

Figure 3, which maximizes between $a_c = 2000 - 4000$. The maximum implies that at this stage, $a_c \cdot 10^{-0.2} < a < a_c \cdot 10^{0.2}$, the growth is modulated statistically strongest by the meteorological conditions.

Note that the different selection of a_c will affect the number of effective sampling countries due to data availability (see the green line in Figure 3). Therefore, we compromise at $a_c = 2000$ so that the correlation coefficient is around the maximum and the amount of samplings is also considerable. Accordingly, we defined $2000 \times 10^{-0.2} < a < 2000 \times 10^{0.2}$ (approximately $1300 < a < 3200$) as the statistical Stage II. In this statistical Stage II, the maximum growth rate $b(a)$ in each country is identified, referred to as the least-constrained growth rate b_m. The red crosses in Figure 2a display b_m of all countries, associated with a median $a = 1424$.

2.4 | The daily growth rate in percentage and its geographical distribution

According to our regression model, the least-constrained growth rate b_m is an exponent and e^{b_m} measures the ratio of the LS-fitted number of confirmed cases of 1 day over that of the previous day. Therefore, $g = \left(e^{b_m} - 1\right) * 100$ is defined as the daily growth rate by percentage. When $b_m \approx 0$, b_m is already a first-order approximation of g due to $g = b_m + \mathcal{O}\left(b_m^2\right) \approx b_m$, since e^b can be expanded into Taylor polynomial $e^b = \sum_{n=0}^{\infty} \frac{b}{n!} = 1 + b + \mathcal{O}\left(b^2\right)$. Here, $\mathcal{O}\left(b^2\right)$ denotes a variable with absolute value at some constant times $|b^2|$ when b is close enough to 0. The following analyses are based on g. The geographical distribution of g is shown in Figure 4.

2.5 | Correlations of the daily growth rate with the meteorological factors

Figure 5 presents the correlation analyses between the least-constrained growth rate g and six meteorological factors, that is, (a) the UV flux in the range of 250–440 nm, (b) the air temperature at 2 m above the surface, (c) the diurnal temperature range, (d) the relative humidity, (e) the wind speed at the height of 10 m, and (f) the precipitation. As an example, Figure S1 displays the UV flux and temperature in Bulgaria. The meteorological factors are extracted from the ERA5 reanalysis at C3S Climate Data Store and sampled and averaged in a 28-day-wide window centring at 7 days before the sampling window centre for fitting the growth rate. The 7-day displacement is used to deal with the COVID-19 incubation period (Lauer et al., 2020). We determine the length of the incubation period in the following subsection. In each panel in Figure 5, one cross denotes one country, corresponding to one red cross

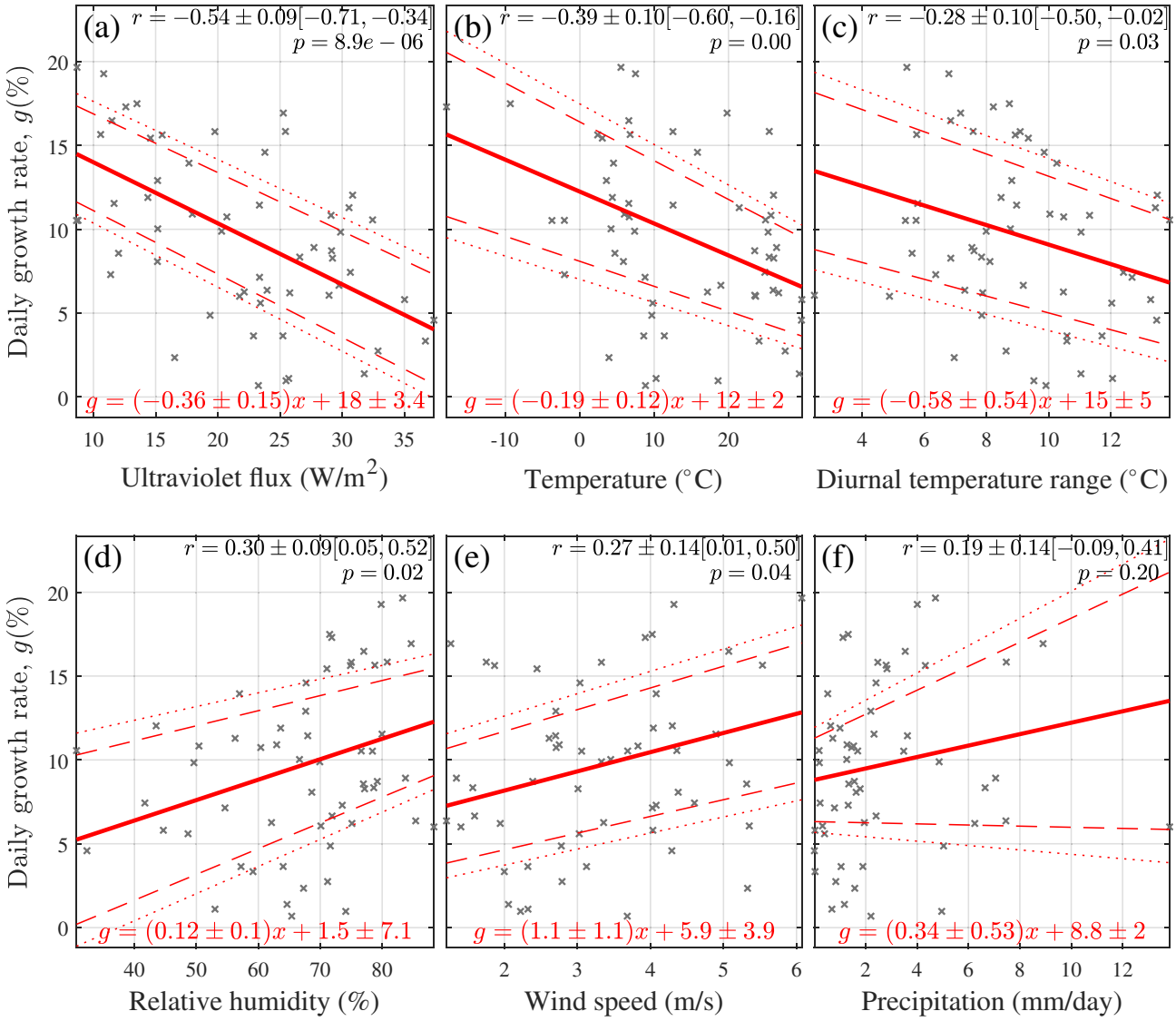

FIGURE 5 Correlation between the daily growth rate g (as defined in Section 2.4) and six meteorological variables: (a) the ultraviolet (UV) flux in the range of 250–440 nm, (b) the air temperature at 2 m above the surface, (c) the diurnal temperature range, (d) the relative humidity, (e) the wind speed at the height of 10 m, and (f) the precipitation. In each panel, one cross represents one country, corresponding to one red cross displayed in Figure 2a; the solid red line presents a robust regression to a linear model $\widehat{g} = \beta_1{}^* x + \beta_0$ through the least absolute deviations method, and the dashed and dotted lines display the significance level $\alpha = 0.05$ and 0.01, respectively. Here, x denotes one of the above six variables, and β_1 and β_0 denote the parameters to be determined. The regression results are displayed in red on the bottom of each panel, while the Pearson correlation coefficient r is printed on the upright corner, in the format of $r \pm \Delta r[r_l, r_u]$. Here, r and Δr are the mean coefficient and its standard deviation estimated through a bootstrapping method, and r_l and r_u are the lower and upper bounds for a 95% confidence interval. Also displayed on the top is the p-value for testing the hypothesis of no correlation.

displayed in Figure 2a. The correlation coefficients and their standard deviation are estimated through a bootstrapping analysis using the Monte Carlo algorithm for case resampling and displayed on the top of each panel. The growth rate exhibits a significant correlation with the UV flux and the air temperature ($r = -0.54 \pm 0.09$ and -0.39 ± 0.10 at $p << 0.01$, in Figure 5a,b, respectively), but not with the other meteorological conditions, namely, wind speed, relative humidity, diurnal temperature range, and precipitation ($p >> 0.05$, Figure 5c–f).

Further, the data points in each panel of Figure 5 are used for a robust regression to a linear model $\widehat{g} = \beta_1{}^* x + \beta_0$ through the least absolute deviations method. Here, x denotes each of the above six variables, and β_1 and β_0 denote the parameters to be determined. The regression results are displayed as red lines in each panel, and the fitted coefficients β_1 and β_0 and their 95% confidence bounds are labelled in red at the bottom of each panel. The regression for the UV reads $\frac{\widehat{g}}{1\%} = (-0.36 \pm 0.15) * \frac{\mathrm{UV}}{1\,\mathrm{W/m^2}} + 18 \pm 3.4$, which reveals that an increase

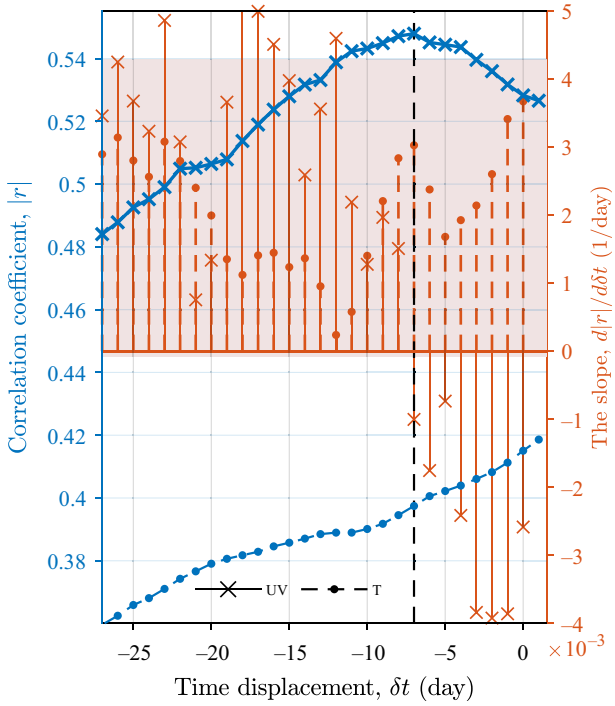

FIGURE 6 The absolute correlation coefficients $|r|$ between the growth rate g and two meteorological factors, the UV flux and temperature T, as functions of the time displacement δt, and their slopes calculated using the centred differencing method. The blue lines denote the correlation coefficients referring to the y-axis on the left whereas the vertical red bars denote their slope referring to the y-axis on the right. The solid lines and bars with crosses denote those associated with the UV flux, whereas the dashed lines and bars with dots denote the results associated with the temperature. The shadow illustrates one standard deviation of the slopes below and above their average. See Section 2.6 for the details.

in UV flux by 1 W/m^2 is associated with a decrease in the growth rate by $0.36 \pm 0.15\%$ per day. The regression for the temperature, $\frac{g}{1\%} = (-0.19 \pm 0.12) * \frac{T}{1^\circ C} + 12 \pm 2$, reveals that an increase of the temperature by 1°C is associated with a decrease in the growth rate by $0.19 \pm 0.12\%$ per day.

2.6 | A cross-correlation analysis suggests an incubation period

The previous subsection uses a time displacement $\delta t = 7$ day between the sampling window of the growth rate and that of the meteorological factors to deal with the incubation period. This incubation period is determined through a cross-correlation analysis. We calculate the absolute correlation coefficient of the growth rate with the UV flux $|r_{UV}|$, as a function of the displacement δt, as displayed in Figure 6.

In Figure 6, $|r_{UV}|$ maximizes at a displacement of 7 days, indicating a 7-day delayed response of the growth to UV flux. A clinical study (Qin et al., 2020) suggested a mean of an incubation period of 6.4 days, while a cross-sectional and a forward follow-up analysis (Lauer et al., 2020) reported a median incubation of 7.76 days. These measures of the incubation period are comparable to the 7-day delay diagnosed herein. Our results provide evidence of the incubation period by analysing confirmed cases instead of controlled experiments from clinical studies.

All results presented above are based on 50% of the most developed countries. For comparison, we conducted the same investigations with data from all countries and found that the incubation period signature weakened (see Figure S2). The weakening could be attributed to the different population density, age distribution and physical characteristics of the population, different socio-economic conditions, and potentially less timely tests in less developed countries (Guha et al., 2020; Khalatbari-Soltani et al., 2020). The delayed tests could reshape the cross-correlation analysis and bias the quantification of the meteorological modulation.

2.7 | On the subjectively defined parameters

In the above analyses, we tried to avoid defining parameters subjectively through, for example, a cross-correlation analysis in determining the incubation, an optimization in determining the centre of Stage II, and replacing the date with confirmed case count in coordinating the Stage II. Even though a couple of parameters are still defined subjectively, including the window width ($\Delta t = 28$ day) used for sliding exponential regression in Section 2.1, the percentage of the 50% of most developed countries in Section 2.2, the half-width of Stage II ($S = 10^{0.2}$) in Section 2.3. These selections are overall compromises among resolution, sampling amount, and significance and robustness of the correlation and regression analyses, similar to the compromise in selecting the Stage centre $a_c = 2000$ in Section 2.6.

Although optimizing each of the above parameters is beyond the scope of the current article, we tested different values of the parameters and produced the same figures as Figures 1–6 but for $\Delta t =$ 16, 20, 24, and 32 days, $S = 10^{0.1}$ and $10^{0.3}$, and $a_c = 1500$, 2500, and 3000, respectively. Although these tests (not shown) resulted in different absolute values of the correlation coefficients, the differences are far less than their uncertainties. Our main conclusions on the correlations and 7-day incubation signature are not subject to our choices of $\Delta t = 28$ day,

$S = 10^{0.2}$, and $a_c = 2000$. We did not test narrower sliding window $\Delta t <$ 16 days because narrower windows might be affected by the artificial weekly periodicity of the confirmed cases associated with the fact that the COVID test capability is more sufficient during working days than during the weekend.

3 | DISCUSSIONS AND CONCLUSIONS

Above we illustrated that the least-constrained growth rate exhibits significant correlations with the meteorological conditions (UV flux and temperature). This finding is in good agreement with previous literature, which highlighted the strong effect of solar irradiance and temperature on the spread of the viruses (Abraham et al., 2021; Isaia et al., 2021) The UV correlation exhibits a delay of about 7 days, which is explained as a signature of the incubation period. Socio-economic factors might modulate the COVID-19 transmission (Guha et al., 2020; Khalatbari-Soltani et al., 2020), which might explain, for example, the distinct difference between east and west Europe in Figure 4, but cannot explain the delay. The temporal variations of socio-economic factors are generally at scales longer than the 7-day delay, which, therefore, can neither modulate the COVID-19 nor respond to the UV flux at 7 days. On the other way around, the presence of the incubation period signature indicates the robustness of the UV modulation on transmission.

There are at least three factors through which meteorological conditions can modulate the transmission. The first is human behaviours. When the temperature is low, humans typically spend more time indoors, with reduced social distancing and less ventilation than outdoors. As an example, schools are places of enhanced influenza transmission (Cauchemez et al., 2008) for intense indoor activities. The second factor is the immune system of susceptible hosts. Solar radiation drives changes in the human immune system by modulating melatonin (Dowell, 2001) and/or vitamin D (Abhimanyu, 2017; Martineau et al., 2017; Whittemore, 2020). Therefore, most respiratory viruses normally exhibit a peak infection during the cold season in densely populated regions (Nittari et al., 2021).

The last but might be the most important factor is the virus's survival, namely the UV's virucidal effect. Evidence has revealed that aerosols are a medium of transmission of COVID-19, as the virus remains active on the surfaces for several hours to days (Liu et al., 2020). Intense solar radiation may inactivate the virus on the surface through physical properties (i.e., shape and size) and the virus's genetic material (Ratnesar-Shumate et al., 2020; Sagripanti & Lytle, 2007; Sutton et al., 2013). Simulation results revealed that 90% of the virus could be inactive in summer daytime for 6 minutes, whereas the virus becomes inactive for 125 min under night conditions (Schuit et al., 2020). In addition, high temperature shortens the virus survival time (Abduljalil & Abduljalil, 2020; Gunthe et al., 2020; Ujiie et al., 2020). On the opposite, low temperature favours prolonging survival on infected surfaces and aerosols, which promotes the diffusion of the infection. The modulation of relative humidity, on the other hand, is negligible, as supported by laboratory experiments (Schuit et al., 2020), which is different from the sensitive modulation on influenza virus survival (Shaman & Kohn, 2009) and transmission (Kudo et al., 2019).

The 7-day-delayed response to the UV flux (Figure 6) reflects the incubation period, whereas the temperature response does not exhibit a delay. A potential explanation is that temperature variation is characterized by a temporal scale longer than the 7-day incubation period, and therefore cannot resolve the incubation period. Another potential explanation is that the temperature might not be an independent drive of the transmission but a response to solar radiation. The temperature correlates significantly with the UV flux ($r = 0.86 \pm 0.03$ at $p = 1.3 \times 10^{-17}$). We carried out a canonical correlation analysis (Seber, 2009) between the growth rate and the UV flux and temperature, resulting in a canonical correlation coefficient $c_{UV,T} = -0.58 \pm 0.08$. The canonical correlation coefficient is close to the UV correlation coefficient $r_{UV} = -0.55 \pm 0.09$ (Figure 5a), which means that using both the UV and temperature as predictors cannot explain more variance than using the UV alone.

The UV impact can drive a seasonality of COVID-19 transmission and explain the following geographic dependence of COVID-19. (1) The mortality exhibits a latitudinal dependence (Whittemore, 2020), with a low UV flux associated with a high growth rate of confirmed cases. (2) The late outbreak in Africa and arid central Asia are attributable to intense UV flux due to the low cloud fraction prior. (3) The onset of the Asian summer monsoon increases clouds in early May (Wang & Ho, 2002) and yields low UV flux, which may account for the late outbreak in India and many southeastern Asia countries until early May. (4) The decrease in UV and temperature during the coming austral winter can contribute to the sharp increase in South America, for example, both the confirmed and dead cases in Brazil ranked second in the world since 13 June, and the transmission enhanced at high latitudes, such as North America and Europe in November 2020.

The current study provides evidence to support the hypothesis that the UV radiation and air temperature

drive the COVID-19 transmission (Whittemore, 2020). Our results also imply a seasonality of COVID-19 and provide a meteorological measure of the incubation period. The virus transmits more readily during winter and during the global monsoon season, which impacts about 70% of the global population (Wang et al., 2017). Accordingly, we predict a high possibility of a resurgence in the boreal winter and suggest adapting the public policy according to the seasonal variability.

AUTHOR CONTRIBUTIONS

Maosheng He: Formal analysis (lead); investigation (lead); methodology (lead); writing – original draft (lead); writing – review and editing (lead). **Keyan Fang:** Conceptualization (lead); data curation (lead); formal analysis (lead); funding acquisition (lead); investigation (lead); methodology (lead); project administration (lead); supervision (lead); writing – original draft (lead); writing – review and editing (lead). **Feifei Zhou:** Data curation (equal); software (equal); validation (equal); writing – original draft (supporting); writing – review and editing (supporting). **Tinghai Ou:** Conceptualization (supporting); data curation (equal); software (equal); validation (equal); writing – original draft (supporting); writing – review and editing (supporting). **Deliang Chen:** Data curation (lead); formal analysis (lead); funding acquisition (lead); methodology (equal); project administration (equal); supervision (lead); writing – original draft (equal); writing – review and editing (lead).

ACKNOWLEDGEMENTS

This study was funded by the National Science Foundation of China (41971022, 41772180 and 41822101), Strategic Priority Research Program of the Chinese Academy of Sciences (XDB26020000). Support from the Swedish Formas (2017-01408) project is also acknowledged. We used the COVID-19 data of cumulative confirmed cases until 1 September of 2020 at a country level from COVID-19 Data Repository by the Center for Systems Science and Engineering (CSSE, https://github.com/CSSEGISandData/COVID-19) at Johns Hopkins University. The daily meteorological variables are extracted from the ERA5 reanalysis at C3S Climate Data Store, see https://doi.org/10.24381/cds.adbb2d47 (C3S, 2017). The gross domestic product per capita 2019 data are downloaded from the World Bank (https://data.worldbank.org/).

ORCID

Maosheng He https://orcid.org/0000-0001-6112-2499

REFERENCES

Abduljalil, J.M. & Abduljalil, B.M. (2020) Epidemiology, genome, and clinical features of the pandemic SARS-CoV-2: a recent view. *New Microbes New Infections*, 35, 100672.

Abhimanyu, A.K. (2017) Coussens, the role of UV radiation and vitamin D in the seasonality and outcomes of infectious disease. *Photochemical & Photobiological Sciences*, 16, 314–338.

Abraham, J., Dowling, K. & Florentine, S. (2021) Can optimum solar radiation exposure or supplemented vitamin D intake reduce the severity of COVID-19 symptoms? *International Journal of Environmental Research and Public Health*, 18, 740.

Anderson, R.M., Anderson, B. & May, R.M. (1992) *Infectious diseases of humans: dynamics and control*. Oxford, England: Oxford university press.

Cauchemez, S., Valleron, A.J., Boëlle, P.Y., Flahault, A. & Ferguson, N.M. (2008) Estimating the impact of school closure on influenza transmission from sentinel data. *Nature*, 452, 750–754.

Dowell, S.F. (2001) Seasonal variation in host susceptibility and cycles of certain infectious diseases. *Emerging Infectious Diseases*, 7, 369–374.

Guha, A., Bonsu, J., Dey, A., & Addison, D. (2020) Community and socioeconomic factors associated with COVID-19 in the United States: zip code level cross sectional analysis. *medRxiv Server for Health Sciences*. [Preprint] p. 2020.04.19.20071944.

Gunthe, S.S., Swain, B., Patra, S.S. & Amte, A. (2020) On the global trends and spread of the COVID-19 outbreak: preliminary assessment of the potential relation between location-specific temperature and UV index. *Journal of Public Health*, 30, 1–10.

Hunt, A.G. (2014) Exponential growth in ebola outbreak since May 14, 2014. *Complexity*, 20, 8–11.

Iqbal, M.M., Abid, I., Hussain, S., Shahzad, N., Waqas, M.S. & Iqbal, M.J. (2020) The effects of regional climatic condition on the spread of COVID-19 at global scale. *Science of the Total Environment*, 739, 140101.

Isaia, G., Diémoz, H., Maluta, F., Fountoulakis, I., Ceccon, D., di Sarra, A. et al. (2021) Does solar ultraviolet radiation play a role in COVID-19 infection and deaths? An environmental ecological study in Italy. *Science of the Total Environment*, 757, 143757.

Kapoor, M., Malani, A., Ravi, S., & Agrawal, A. (2020) Authoritarian governments appear to manipulate COVID data. *arXiv: 2007.09566*. [Preprint].

Khalatbari-Soltani, S., Cumming, R.C., Delpierre, C. & Kelly-Irving, M. (2020) Importance of collecting data on socioeconomic determinants from the early stage of the COVID-19 outbreak onwards. *Journal of Epidemiology and Community Health*, 74, 620–623.

Kudo, E., Song, E., Yockey, L.J., Rakib, T., Wong, P.W., Homer, R.J. et al. (2019) Low ambient humidity impairs barrier function and innate resistance against influenza infection. *Proceedings of the National Academy of Sciences of the United States of America*, 166, 10905–10910.

Lai, S., Ruktanonchai, N.W., Zhou, L., Prosper, O., Luo, W., Floyd, J.R. et al. (2020) Effect of non-pharmaceutical interventions to contain COVID-19 in China. *Nature*, 585, 410–413.

Lauer, S.A., Grantz, K.H., Bi, Q., Jones, F.K., Zheng, Q., Meredith, H. R. et al. (2020) The incubation period of coronavirus disease 2019 (COVID-19) from publicly reported confirmed cases: estimation and application. *Annals of Internal Medicine*, 172, 577–582.

Liu, Y., Gayle, A.A., Wilder-Smith, A. & Rocklöv, J. (2020) The reproductive number of COVID-19 is higher compared to SARS coronavirus. *Journal of Travel Medicine*, 27, taaa021.

Maier, B.F. & Brockmann, D. (2020) Effective containment explains subexponential growth in recent confirmed COVID-19 cases in China. *Science (80)*, 368, 742–746.

Martineau, A.R., Jolliffe, D.A., Hooper, R.L., Greenberg, L., Aloia, J.F., Bergman, P. et al. (2017) Vitamin d supplementation to prevent acute respiratory tract infections: systematic review and meta-analysis of individual participant data. *BMJ*, 356, i6583.

Nittari, G., Marino, P., Gibelli, F., Sossai, P., Sirignano, A. & Ricci, G. (2021) Role of meteorological factors in the spread of the severe acute respiratory syndrome coronavirus 2 (SARS-CoV-2) pandemic in Italy. *European Review for Medical and Pharmacological Sciences*, 25, 7135–7143.

Picoli Junior, S.d., Teixeira, J.J.V., Ribeiro, H.V., Malacarne, L. C., Santos, R.P.B.d. & Mendes, R.d.S. (2011) Spreading patterns of the influenza A (h1n1) pandemic. *PLoS One*, 6, 1–4.

Qi, H., Xiao, S., Shi, R., Ward, M.P., Chen, Y., Tu, W. et al. (2020) COVID-19 transmission in mainland China is associated with temperature and humidity: a time-series analysis. *Science of the Total Environment*, 728, 138778.

Qin, J., You, C., Lin, Q., Hu, T., Yu, S. & Zhou, X.-H. (2020) Estimation of incubation period distribution of COVID-19 using disease onset forward time: a novel cross-sectional and forward follow-up study. *Science Advances*, 6, eabc1202.

Ratnesar-Shumate, S., Williams, G., Green, B., Krause, M., Holland, B., Wood, S. et al. (2020) Simulated sunlight rapidly inactivates SARS-CoV-2 on surfaces. *The Journal of Infectious Diseases*, 222, 214–222.

Sagripanti, J.L. & Lytle, C.D. (2007) Inactivation of influenza virus by solar radiation. *Photochemistry and Photobiology*, 83, 1278–1282.

Sajadi, M.M., Habibzadeh, P., Vintzileos, A., Shokouhi, S., Miralles-Wilhelm, F. & Amoroso, A. (2020) Temperature, humidity, and latitude analysis to estimate potential spread and seasonality of coronavirus disease 2019 (COVID-19). *JAMA Network Open*, 3, e2011834.

Schuit, M., Ratnesar-Shumate, S., Yolitz, J., Williams, G., Weaver, W., Green, B. et al. (2020) Airborne SARS-CoV-2 is rapidly inactivated by simulated sunlight. *The Journal of Infectious Diseases*, 222, 564–571.

Seber, G.A.F. (2009) *Multivariate observations*, Vol. 252. Hoboken, NJ: John Wiley & Sons.

Shaman, J. & Kohn, M. (2009) Absolute humidity modulates influenza survival, transmission, and seasonality. *Proceedings of the National Academy of Sciences*, 106, 3243–3248.

Sutton, D., Aldous, E.W., Warren, C.J., Fuller, C.M., Alexander, D.J. & Brown, I.H. (2013) Inactivation of the infectivity of two highly pathogenic avian influenza viruses and a virulent Newcastle disease virus by ultraviolet radiation. *Avian Pathology*, 42, 566–568.

Tian, H., Liu, Y., Li, Y., Wu, C.H., Chen, B., Kraemer, M.U. et al. (2020) An investigation of transmission control measures during the first 50 days of the COVID-19 epidemic in China. *Science (80)*, 368, 638–642.

Ujiie, M., Tsuzuki, S. & Ohmagari, N. (2020) Effect of temperature on the infectivity of COVID-19. *International Journal of Infectious Diseases*, 95, 301–303.

Wang, B. & Ho, L. (2002) Rainy season of the Asian-Pacific summer monsoon. *Journal of Climate*, 15, 386–398.

Wang, P.X., Wang, B., Cheng, H., Fasullo, J., Guo, Z.T., Kiefer, T. et al. (2017) The global monsoon across time scales: mechanisms and outstanding issues. *Earth-Science Reviews*, 174, 84–121.

Whittemore, P.B. (2020) COVID-19 fatalities, latitude, sunlight, and vitamin D. *American Journal of Infection Control*, 48, 1042–1044.

Yao, Y., Pan, J., Liu, Z., Meng, X., Wang, W., Kan, H. et al. (2020) No association of COVID-19 transmission with temperature or UV radiation in Chinese cities. *The European Respiratory Journal*, 55, 2000517.

SUPPORTING INFORMATION

Additional supporting information can be found online in the Supporting Information section at the end of this article.

How to cite this article: He, M., Fang, K., Zhou, F., Ou, T., & Chen, D. (2022). A delayed modulation of solar ultraviolet radiation on the COVID-19 transmission reflects an incubation period. *Meteorological Applications*, *29*(5), e2099. https://doi.org/10.1002/met.2099